Results of a search for annual modulation of WIMP signals

M. L. Sarsa, A. Morales, J. Morales, E. García, A. Ortiz de Solórzano, J. Puimedón, C. Sáenz, A. Salinas, and J. A. Villar
Laboratory of Nuclear and High Energy Physics, University of Zaragoza, 50009 Zaragoza, Spain
(Received 20 January 1997)

A search for particle cold dark matter (CDM) has been carried out at the Canfranc Underground Laboratory (Spain) with a set of three sodium iodide scintillators of 10.7 kg each, during about 2 yr of data taking. The results, corresponding to an exposure of 4613.6 kg day are presented in the form of exclusion plots of the WIMP-target nuclei cross section versus WIMP mass (both for spin-independent and spin-dependent WIMP-matter interactions), obtained with the standard method of comparing the observed rate with the expected signal. A distinctive feature of the CDM signal, like its expected annual modulation, has also been looked for in 1342.8 kg day of data. The nonobservance of such a modulation has been used to draw more stringent exclusion plots than those derived from the standard method. [S0556-2821(97)02316-3]

PACS number(s): 95.35.+d, 14.60.St, 29.40.Mc

I. INTRODUCTION

Cold dark matter (CDM) particles such as weakly interacting massive particle (WIMP's), hypothetically forming a large fraction of the galactic halo, could be detected in the laboratory through the nuclear recoil produced by their elastic scattering off target nuclei, like those forming the material of solid or liquid scintillators. The 100% isotopic contents on A-odd isotopes of NaI scintillators (^{127}I and ^{23}Na, respectively), which make them sensitive to spin-dependent interactions with WIMP's, have prompted the development of low background NaI scintillators for CDM searches [1–3].

We present in this paper the results of a search for WIMP's performed with a set of sodium iodide scintillators and draw the regions of WIMP masses and cross sections which are excluded by this experiment. The exclusion plots are derived, as customary, by comparing the predicted CDM signal with the total number of counts recorded experimentally in a given energy region. It is a common prejudice that this conventional method will not likely detect the tiny WIMP signal, but only exclude it or constrain its properties. A convincing proof of the detection of CDM would be to find unique signatures in the data, characteristic of the CDM, which cannot be faked by the background or by instrumental artifacts.

Distinctive features of the C.D.M. signal, like its annual [4] modulation, are expected to provide unequivocal identification of the elusive WIMP's. The first result ever published of a search for such a modulation appeared some time ago [5] and was performed with a Ge detector in the Canfranc tunnel. The present work reports on the results of a search for annual modulation effects in the spectra recorded with a set of scintillators. The data taking of this experiment extends over a period of about 2 yr, with a total mass of 32.1 kg of sodium iodine crystals, in an underground location at 675 m.w.e. (meters of water equivalent). The exposure used in the analysis to derive exclusion plots from the total observed rate by comparing it with the expected signal refers to 4613.6 kg day. To analyze the seasonal modulation 1342.8 kg day of data, corresponding to the exposures of June minus December in 2 yr, have been used. The data do not show any difference between the rates of June and December (within a given confidence level), as one would expect from the faster relative velocity Earth-halo in June than in December. A complementary analysis intended to discover a possible periodic component in the data (the so-called modulation significance method [6]) gives a null result. The absence of such modulation effect results in constraints on masses and cross sections of spin-dependent and spin-independent interactions of WIMP's which are more stringent than that obtained from the customary method of comparing the expected rate with that recorded in a given energy region.

II. EXPERIMENTAL SETUP

The detector is a set of three NaI scintillators made by BICRON. Each crystal (regular hexagonal cross section of 8.0 cm each side and height of 20.3 cm) has a mass of 10.7 kg. The crystals are encapsulated in stainless steel 304 L, 0.5 mm thick, and coupled to photomultipliers EMI9765 by a (7.62 cm diameter) quartz window. The shielding consists of 20 cm of low activity lead and inner OFHC (oxygen-free high conductivity) copper sheets ($\sim$6 mm thickness). A PVC box (silicone sealed) tightly closes the shielding and is surrounded by 1 mm of cadmium and 20 cm of paraffin and borated polyethylene. All the shielding and mounting is supported by 10 cm of vibrational and acoustic insulator sandwiched between two layers of 10-cm wood mounted on a 20-cm concrete floor (Fig. 1). The experimental setup was placed in the Underground Laboratory of the University of Zaragoza, at the Canfranc Tunnel (Spanish Pyrenees) at a depth of 675 m.w.e. The measured muon flux at the site of the experiment was $\Phi = 4 \times 10^{-6}$ cm^{-2} s^{-1}.

Radon removal was achieved by pressurizing the inner cavity with forced-evaporating liquid nitrogen (appox. 60 l per h). The radon removal has resulted in about a 50% reduction in the total rate of events. The effect of the disappearance of the N_2 overpressure can be seen in Fig. 2. The radon gas reaches its equilibrium inside the cavity (after difunding through the shielding) after about 20 h. From the comparison of the spectra obtained with and without the N_2 overpressure, the ^{222}Rn contamination in the air of our un-

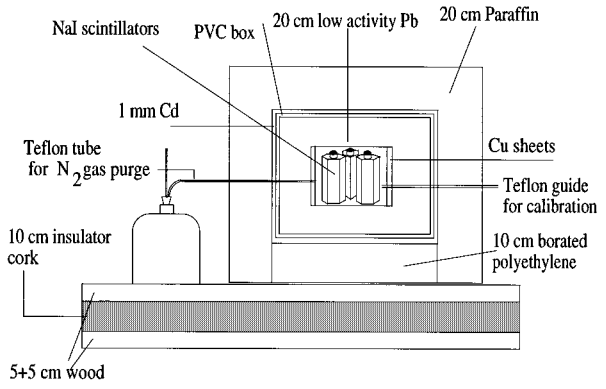

FIG. 1. Schematic view of the experimental setup.

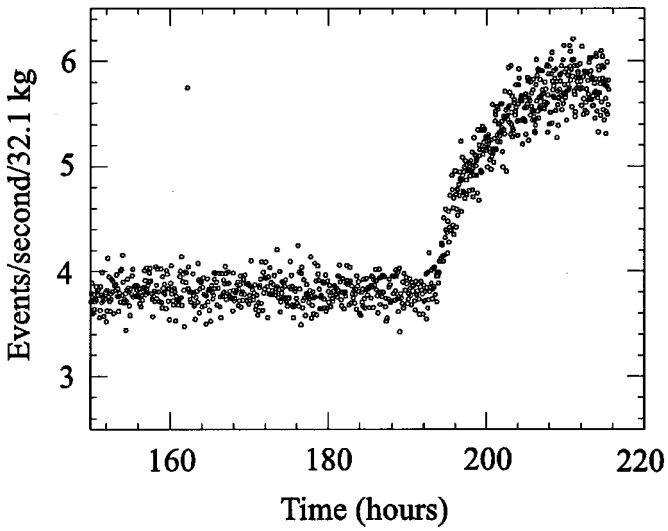

FIG. 2. Effect of the disappearance of the N_2 overpressure in the total events rate of the experiment. A 50% of reduction is achieved by means of this radon removal.

derground laboratory has been estimated to be ~ 1.6 pCi per l.

Readout electronics (see Fig. 3) consists of a fast-slow coincidence system based on standard NIM modules. The fast signals pass through fast amplifiers (TFA's) and timing single-channel analyzers (TSCA's). The fast-negative NIM logic signals are sent to a coincidence module working with multiplicity $M \geqslant 1$. The logic output signal is used to generate (in a Window Generator) a slow-positive NIM signal which is sent to a scale (to register the total event rate) and is used as the GATE signal on the analogue-to-digital converters (ADCs). The slow branch consists of spectroscopy linear amplifiers and analogue-to-digital converters. The digital output lines are connected through an interface module to a PC-Lab 720 II-A parallel digital I/O & Counter card installed on a PC computer. The ADC's work in the LATE Coincidence mode with a linear gate time of 15 μs and gated by the Window Generator output. Data from the converters are read when one of the ADC's fires. For each event, the multiplicity, arrival time, and energies of the ADC's with DATA READY signal are recorded. The total event rate registered in the experiment was 3.1 events per s (after the copper foil installation). Overall deadtime of the experiment (including detectors, electronics, and acquisition software) has been estimated to be approximately 450 μs per event, which represents less than 0.2% of the measuring time.

Coincidences between two or three detectors were removed by software because their origin is certainly not a CDM signal. The rate of coincidences was approximately 0.13 coincidences per s. Thus, removal of the coincidences gives rise to a 4% reduction in the data.

As is customary, events arriving in bursts were also removed. Figure 4 shows that they do not follow a Poisson statistics and can be safely rejected. In particular, bursts of seven or more events in an interval of 0.05 s were rejected. Assuming that the background of the experiment follows a Poisson distribution, with our average counting rate ($3.1\ s^{-1}$) the probability of having such bursts is smaller than 5×10^{-8}. Thus, no appreciable reduction of the counting time is produced. Our electronic system and antivibratory

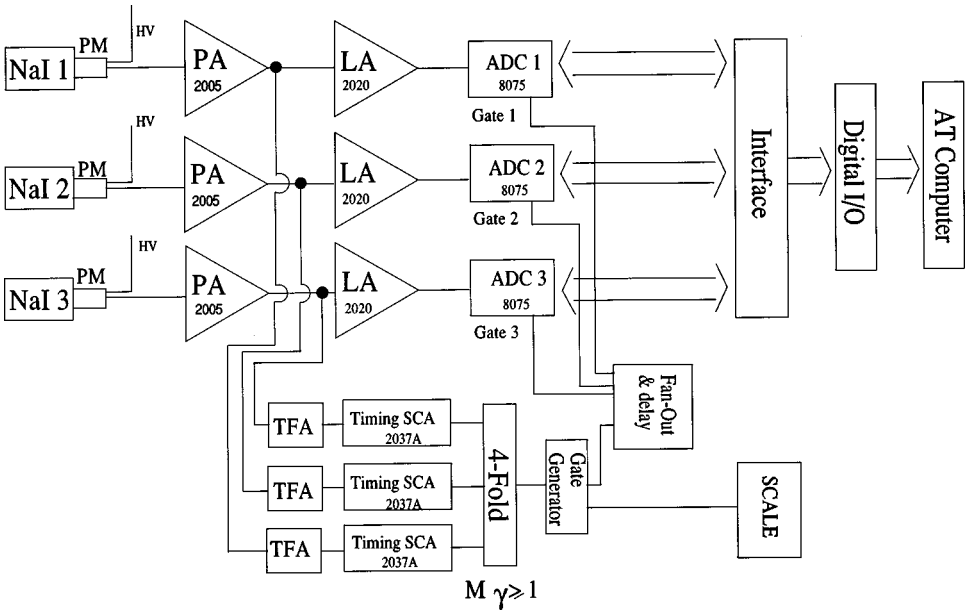

FIG. 3. Schematic view of the electronic acquisition system.

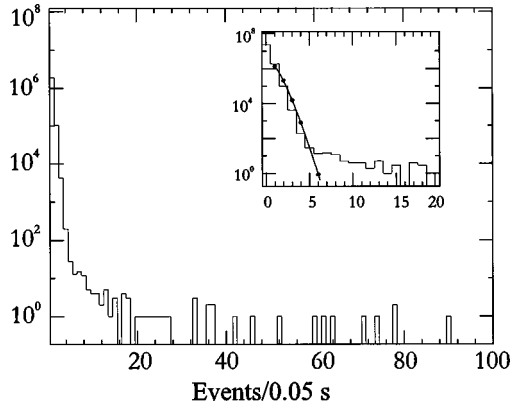

FIG. 4. Experimental distribution of the events which arrive within 0.05 s compared with the expectation for a Poisson statistics.

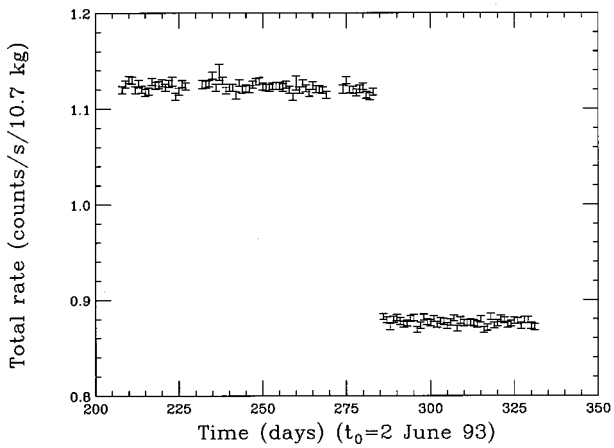

FIG. 5. Reduction in the total events rate after placing copper inside the shielding.

platform contributed also to reducing the usual microphonic noise.

An important improvement in the background of the low-energy region (equivalent to a 20% of reduction in the corresponding total rate) resulted from the installation of copper sheets between the detectors and the lead (see Fig. 5). This reduction corresponds basically to the disappearance of the x rays from lead, coming from the external shielding, but also to a continuum up to 1 MeV. However, the nondisappearance of the 46.5 keV peak (see Fig. 6) shows that the corresponding ^{210}Pb contamination is not in the lead shielding, but in the detectors themselves. As stated above the inner shielding of the experimental setup included the OFHC copper sheets.

Figure 6 shows the recorded spectrum for $Mt = 4613.6$ kg day used in the data analysis (continuous line) and that obtained prior to the inclussion of the thin copper sheets (dashed line). The peak appearing in the very low-energy region of the spectrum has been assigned to the escape of an x ray of iodine after photoelectric absorption of the 46.5-keV γ and x_L rays from bismuth following the internal conversion of the 46.5-keV level. That would imply that the ^{210}Pb contamination lies close to the crystal surface and that the ^{210}Bi electrons and bremsstrahlung (end point 1.16 MeV) can contribute to the spectrum. According to Monte Carlo (MC) simulations which have tried various locations for the ^{210}Pb contaminant, one is able to reproduce fairly well the low-energy region of the observed spectrum by assuming that the ^{210}Pb is contained within the iron caps of the NaI crystals in an amount of about 4 Bq kg^{-1} (or in the crystal surface as radon deposition) plus a 10–16 Bq kg^{-1} content in the photomultipliers components. Other experiments with the same kind of scintillators have also reported ^{210}Pb contaminations [2,3].

Figure 7 shows the main contributions to the total background spectrum. The main peaks in the low-energy region are those of ^{210}Pb and the lead x rays. At higher energies the principal contributions are due to the ^{60}Co (in the steel components) and to the ^{40}K (in the crystals) contaminations as well as to the natural radioactivity chains (^{232}Th mainly). Table I quotes the contribution to the photopeak of the main background contaminants. In addition to the ^{210}Pb nearby the crystals, another important part of the continuum of the scintillator spectra arises from an internal contamination in ^{40}K, which is also a β-decaying isotope. This contamination (according to MC estimates of the efficiency for detecting the 1460.8-keV γ rays and the observed rate at this line) should be smaller than 20 mBq kg^{-1} (taking into account that a part of this contaminant could be accounted for in the PM's). Similar amounts of ^{40}K in the NaI crystals were reported in other NaI dark matter experiments [1] where the internal-external contributions could be dissentangle by using pulse analysis discrimination.

Other experimental parameters of this experiment are as follows: The overall energy resolution is 9% at 511 keV and 30% at 46.5 keV. The energy threshold is about 8 keV of visible energy and the differential rate at the energy windows used in the CDM analysis (from 9 to 28 keV) ranges from 16 to 8 counts keV^{-1} kg^{-1} day^{-1}. Over the total measuring time, the stability achieved has been 0.6% at the 661.6-keV ^{137}Cs calibration peak, and 2 and 1.2 % at the ^{40}K and ^{210}Pb background lines, respectively.

The calibration of the 4613.6 kg day final spectrum has been performed by combining peaks obtained every week with different radioactive sources (^{137}Cs, ^{60}Co, and ^{22}Na)

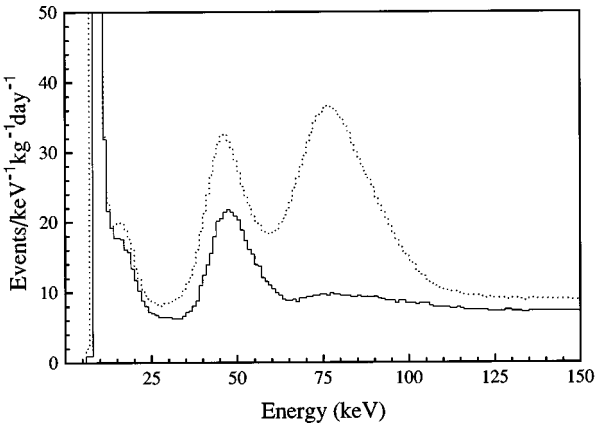

FIG. 6. Spectrum with (solid line) and without (dotted line) a thin internal copper liner in the shielding normalized to events keV^{-1} kg^{-1} day^{-1}. The solid line spectrum, corresponding to an exposure of 4613.6 kg day, has been used to derive the exclusion plots in the conventional method of confronting expected signal to observed background rate.

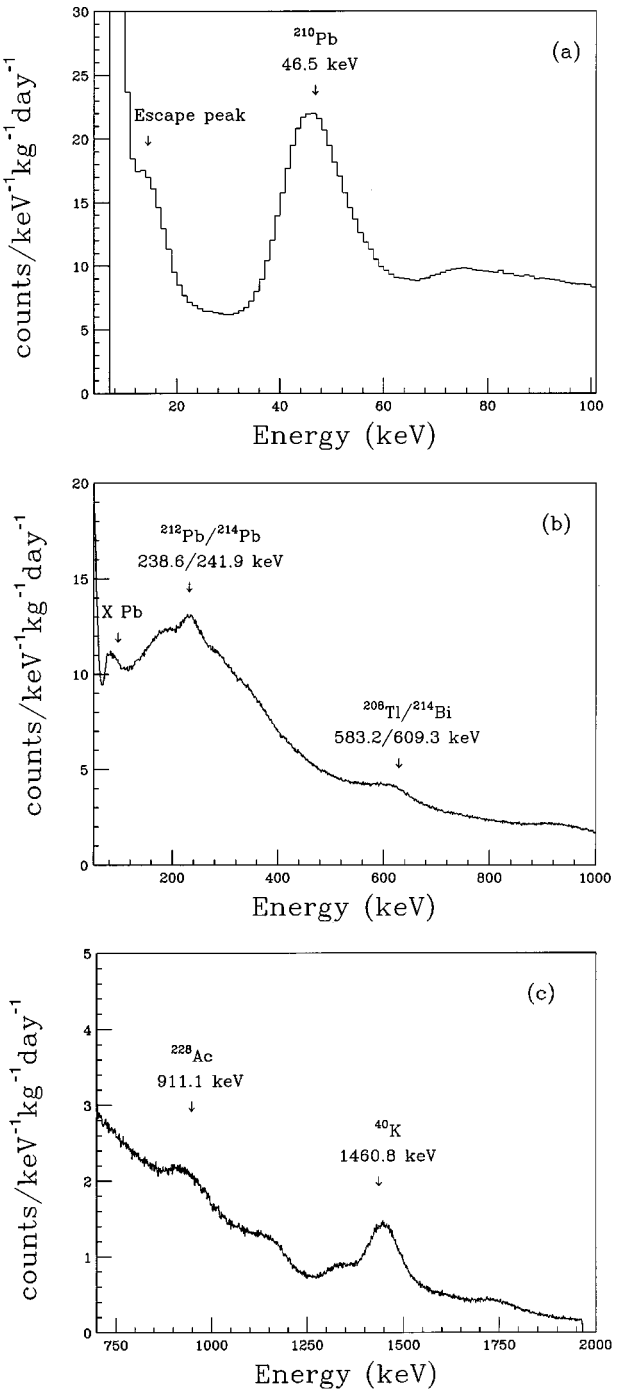

FIG. 7. Background of the scintillators in the best conditions found along the experiment. The most relevant contaminants are ^{40}K, ^{210}Pb, ^{232}Th, and ^{238}U.

and standard background lines clearly identified in the spectrum (taking advantage of the stability of the experiment). In particular, the low-energy region (below 100 keV) has been calibrated by using the ^{210}Pb peaks and the *K*-shell x rays of lead and barium produced in the weekly calibration with the ^{137}Cs radioactive source.

III. RESULTS OF A CONVENTIONAL DARK MATTER SEARCH

The expected rate for WIMP-nuclei interactions, computed in the usual way [7,8], is given by

TABLE I. Contribution to the photopeak of the main background contaminants.

Contaminant	Contribution (events day^{-1})
^{210}Pb (46.5 keV)	$2.16(\pm 0.43)\times 10^3$
^{40}K (1460.8 keV)	$1.04(\pm 0.17)\times 10^3$
^{208}Tl/^{214}Bi (583.2/609.3 keV)	$0.52(\pm 0.09)\times 10^3$

$$\frac{dN}{dtdT} = N_n \frac{\rho}{m} \int \frac{d\sigma}{dT} f(\vec{v}) v d^3v,$$

where T is the recoil energy of the target nuclei, $f(\vec{v})$ is the velocity distribution of the halo's WIMP's in the reference frame of the Earth, N_n is the total number of target nuclei per, say, kilogram, ρ is the local galactic halo density, m is the WIMP mass, and $d\sigma/dT$ is the differential scattering cross section. The measured (electron equivalent or visible) energy E is related to the nuclear recoil energy T by the relative efficiency factor Q, $E=QT$ (nuclear versus electron recoil efficiency in producing ionization). The values used in this work are $Q(^{23}\mathrm{Na})=0.4\pm 0.2$ and $Q(^{127}\mathrm{I})=0.05\pm 0.02$, taken from Ref. [3]. There exist other experimental values of Q for these nuclei [9–11], but they are compatible within errors. The integral goes from $v_{\min}(T)$—minimum relative velocity the WIMP must have in order to leave an energy T in the detector, i.e., $v^2_{\min}=T\,(M+m)^2/2\,m^2M$, where M is the target nucleus mass—up to $\vec{v}_{\max}$, which is the maximum velocity of the WIMP relative to the detector, i.e., the vectorial sum of the galactic escape velocity $\vec{v}_{\mathrm{esc}}$ and that of the Earth through the halo $\vec{v}_r$. As customary, it has been assumed that the dark matter forms a nonrotating, isothermal and spherically symmetric halo. In the galactic rest frame, the WIMP's are supposed to have a Maxwellian velocity distribution, with a velocity dispersion v_{rms}, which in this work we have assumed to be 270 km s^{-1}. The escape velocity for the WIMP's in the halo, the value of which ranges from 650 to 1300 km s^{-1}, has been set to infinite. For the Earth-halo relative velocity we have taken as value 232 km s^{-1}. The local halo density has been taken $\rho = 0.3$ GeV cm^{-3}, with the caution that this value could have an uncertainty of a factor 2. It is a well-known fact that the subsequent dependence of the rate on these parameters is a serious shortcoming of this type of calculation.

In our case the expected WIMP signal in counts per keV per kilogram and day is given by

$$S = 7.76\times 10^{14} N_n \frac{1}{Q} \frac{(m+M)^2}{4Mm^3} \sigma_w \rho \frac{\eta}{v_r},$$

where σ_w is the elastic cross section of the WIMP-nucleus interaction (in cm^2), which includes the form-factor correction for high momentum transfer, $\sigma_w=\sigma_p F^2(T)$, σ_p being the pointlike cross section, given, respectively, for coherent and spin-dependent interactions by

$$\sigma_p^{\mathrm{SI}} = \frac{G_F^2}{8\pi} \mu^2 [(1-4\sin^2\theta_w)-N]^2$$

and

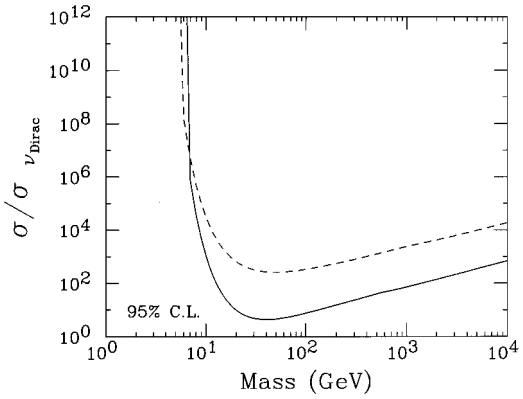

FIG. 8. Exclusion plots for coherent interactions in units of the Dirac neutrino cross section obtained by comparing the predicted signal with the observed background (dashed line) and with the annual modulation search (solid line).

$$\sigma_p^{\mathrm{SD}}=\frac{G_F^2}{8\pi}\,\mu^2\lambda^2 J(J+1)$$

(pointlike cross section for Dirac and Majorana neutrinos). $\mu=mM/(m+M)$ is the reduced mass WIMP-target nuclei, G_F the weak-coupling constant $G_F=1.023\times10^{-5}\ m_p^{-2}$, and θ_w the Weinberg angle. Masses are expressed in GeV.

The integral over the velocity distribution in the assumed case of an infinite escape velocity appears through the function η given by

$$\eta=\mathrm{erf}(x+y)-\mathrm{erf}(x-y),$$

where

$$x=\sqrt{3/2}v_{\min}/v_{\mathrm{rms}},$$

$$y=\sqrt{3/2}v_r/v_{\mathrm{rms}},$$

and erf(z) the usual error function [(erf(z) $=(2/\sqrt{\pi})\int_0^z\exp(t^2)dt$)]

The exclusion plots have been derived by requiring that the predicted signal cannot be larger than the upper limit of

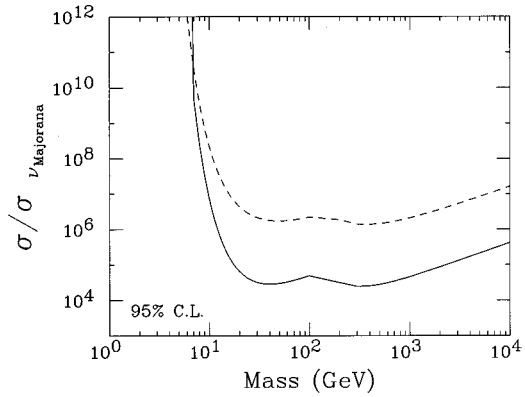

FIG. 9. Exclusion plots for spin-dependent interactions in units of the Majorana neutrino cross section obtained by comparing the predicted signal with the observed background (dashed line) and with the annual modulation search (solid line). Two different energy windows have been used.

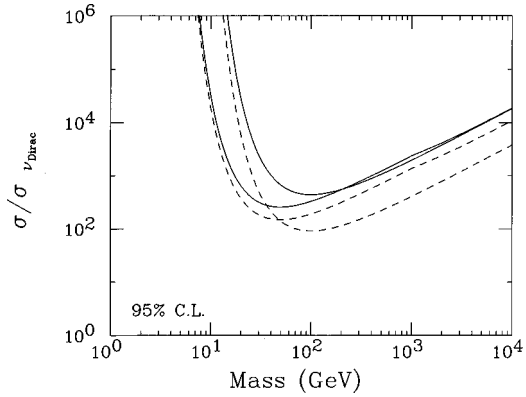

FIG. 10. Exclusion plots for coherent interactions in units of the Dirac neutrino cross section obtained by comparing the predicted signal with the observed background with (dashed line) and without (solid line) background modeling. Two different energy windows have been used.

counts in a Poisson process in which B counts are observed. The counts refer to a given energy bin of a width not too different from that of the energy resolution. The bin has been chosen from 9 keV to 17 keV but other nearby regions lead to similar results. We have followed the conservative criterion of choosing, for the analysis, energy regions of width suggested by the energy resolution of the NaI. The $\sigma(m)$ bounds (at 95% C.L.) are shown as a dashed line in Figs. 8 and 9, for, respectively, the coherent and spin-dependent cases, and have been derived from the solid line spectrum of Fig. 6. The plotted cross sections are pointlike. The corresponding coherent and spin nuclear form factors were taken into account in the derivation of the rates, assuming Fermi form factors for the coherent case. For the spin case, unity has been taken for ^{23}Na whereas for ^{127}I we have assumed the same as for ^{131}Xe [12]. The $\lambda^2\ J\ (J+1)$ factors for ^{23}Na and ^{127}I are, respectively, as taken in the odd group model 0.041 [13] and 0.023 [14]. No background subtraction has been done in deriving the exclusion plots from the spectrum of Fig. 6 ($Mt=4613.6$ kg day).

Should one have used as a statistical estimator the upper limit of counts in a Poisson process with background (that

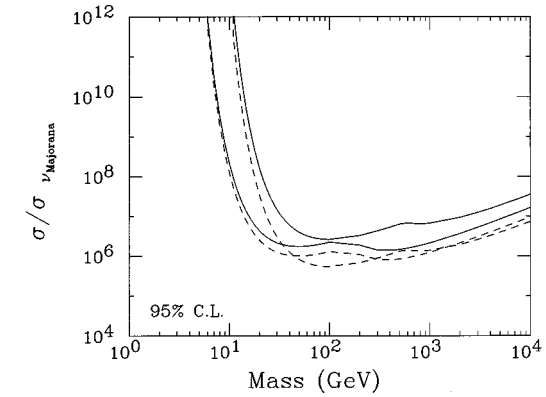

FIG. 11. Exclusion plots for spin-dependent interactions in units of the Majorana neutrino cross section obtained by means of conventional techniques with (dashed line) and without (solid line) background modeling. Two different energy windows have been used.

due to ^{210}Pb and ^{40}K, as obtained from the corresponding MC simulations), one would have obtained the exclusion plot corresponding to the dashed lines depicted in Fig. 10 (for spin-independent interactions). In much the same way, Fig. 11 depicts both cases for spin-dependent interactions. For comparison with results from other target nuclei we have normalized in the plots the pointlike cross sections to that of Dirac and Majorana neutrino ones.

IV. RESULTS OF THE ANNUAL MODULATION SEARCH

The yearly modulation [4] is originated because of the seasonal variation in the relative velocity of the Earth and the galactic halo due to the Earth's rotation around the Sun. The Sun moves around the galaxy at a velocity of 232 ± 20 km s^{-1}, and the Earth moves around the Sun with an orbital speed of 30 km s^{-1} in an orbit whose axis makes an angle of $\delta = 30.7°$ with respect to the vector velocity of the Sun. The time dependence of the relative velocity Earth-halo is expressed by $v_r(t) = v_\odot + v_\oplus \sin\delta \cos[\omega(t-t_0)]$, where $\omega = 2\pi/365$ (day^{-1}). The time t_0 corresponds to June 2nd, where the projection of the Earth velocity onto the Sun one is maximum. The resulting net speed of the Earth with respect to the halo's reference frame oscillates between about 245 km s^{-1} in June and 215 km s^{-1} in December, and so the maximum amount of energy that can be deposited by the WIMP's in the detector, as well as their detection rates change accordingly, and so an annual modulation of the dark matter signal should appear.

The dimensionless Earth-halo relative velocity $y(t)$ is expressed as $y(t) = y_0 + \Delta y \cos[\omega(t-t_0)]$, where $y_0 = 1.05$ and $\Delta y = 0.07$ according to our choice of velocity values. The expected modulated signal accordingly can be expressed, in first order, as a constant term plus a modulation component of amplitude S_m, $S(t) = S_0 + S_m \cos[\omega(t-t_0)]$, where $S_m = [\partial S/\partial y]_{y0} \Delta y$. The modulation is expected to be small (a few percent) compared to the total DM signal.

The amplitude of the modulated term S_m is depicted in Figs. 12(a) and 12(b) for Dirac neutrinos of masses ranging from 1 GeV to 1 TeV in the case of interactions in sodium [Fig. 12(a)] and in iodine [Fig. 12(b)]. The relevant role of the target nucleus mass in the interaction rates should be emphasized: for sodium the rates are lower over a wide energy range, whereas for iodine, high rates can be achieved for very low visible energy.

To search for the existence of a modulation in the data, one could either simply look for a difference between the rates of June and December or to extract the possible periodic component of the data (if any) overimposed to a large random component by means of a cosine transform, as suggested in Ref. [6].

We have analyzed first the annual modulation through the June minus December experimental residual and derived the exclusion plots $\sigma(m)$ obtained by comparing it with what was to be expected. Data recorded with the three NaI detectors during two years (1993 and 1994), integrated in an interval of a month around these maxima (June 2) and minima (Dec. 4), have been used, corresponding to an effective exposure of 1342.85 kg day. Figure 13 shows the corresponding residuals, compared with the theoretically expected signals from two CDM candidates (a WIMP of 150 GeV and

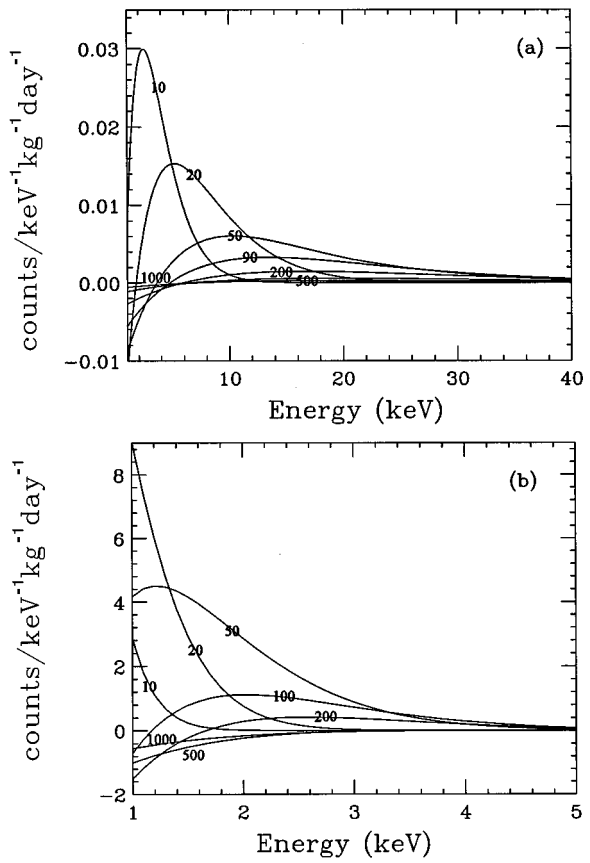

FIG. 12. Modulation amplitude of Dirac neutrinos of masses ranging from 1 GeV to 1 TeV interacting with sodium (a) and iodine (b) (masses are labeled in GeV).

$\sigma = 10^{-30}$ cm^2 interacting with I—solid line—and one of $m = 30$ GeV and $\sigma = 10^{-32}$ cm^2 interacting with Na—dotted line). The exclusion plots are shown in Figs. 8 and 9 as a solid line. The improvement in sensitivity obtained with the annual modulation search (time variation of the rate) with respect to that of the conventional (total rate) method is clearly seen. As expected from well-known arguments the

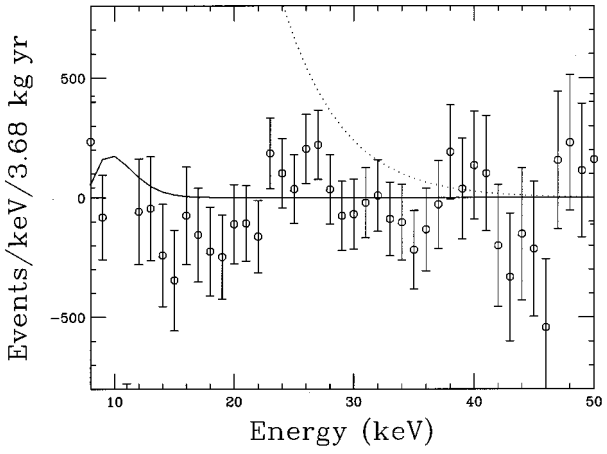

FIG. 13. June minus December spectra. The expected residual signal for typical WIMP's are also shown: $M = 30$ GeV and $\sigma_{Na} = 10^{-32}$ cm^2 (dotted line) and $M = 150$ GeV and $\sigma_I = 10^{-30}$ cm^2 (solid line).

TABLE II. Value of the parameters of the modulation significance analysis.

Energy window (keV)	x	r	C.L.
10–18	0.067	0.0136	0.5054
20–28	0.059	0.0176	0.5068

improvement in sensitivity with increasing statistics is faster when analyzing residuals (like June minus December) than when using the total spectrum. For comparison with other experiments see [1–3] (NaI scintillators) and [8,15–18] (Ge detectors).

The second procedure mentioned above [6] follows the well-known strategy of projecting out a possible periodic component by Fourier or cosine transforming the data. This is accomplished in Ref. [6] by using as an indicator of the modulation the modulation significance defined as $R=X/\sigma(X)$ where $X=\Sigma 2\cos(\omega t_i)[S(t_i)+B(t_i)]$. $S(t_i)$ and $B(t_i)$ are Poisson random variables representing, respectively, the signal and background data collected in a time bin of 1-day width centered at time t_i. For our particular experiment, a measure of R is given by $r=x/\sqrt{4\alpha d}$ where x is measure of X and d a measure of $\Sigma S(t_i)+B(t_i)$, α is a correction factor [6] to account for the fact that we do not have data all the days of the year ($\alpha=0.607$).

For the modulation significance analysis, we have used data of only two NaI detectors (21.4 kg) and a total of 424 days (paired, i.e., opposite in the cosine period). Table II shows the value of modulation significance r and its related confidence level for the two energy windows used in this analysis. Also the value of the random variable x (where $\langle x\rangle=2\alpha TS_m$) is given. If there is no modulation, r is Gaussian distributed around zero, with $\sigma=1$. The confidence level for a measured value r_0 of R to indicate the existence of a signal modulation is $CL=1/2+1/2\mathrm{erf}(|r_0|/\sqrt{2})$. A value $r_0=1.28$ (i.e., 90% C.L.) would be a fair indication of the existence of an annual modulation, whereas no modulation would correspond to a C.L. of 50%. To conclude about the possible existence of a modulation, one should perform the modulation significance analysis in various energy windows and checked it by looking also at the modulation component orthogonal to x [same as r but with $\sin(\omega t_i)$ instead of $\cos(\omega t_i)$]. The presence of a signal modulation in the data should show up in both distributions of the values of r and s, which, for no modulation, are both random variables with zero mean and unit variance. The results shown are compatible with the absence of modulation. This absence could be expressed as an upper bound (at a given C.L.) for the modulated term. The constraints in the $\sigma(m)$ plots drawn in Figs. 8 and 9 have been obtained instead through the June minus December method.

V. CONCLUSIONS

We have performed an experiment intended to look for WIMP's through their elastic scattering off sodium and iodine nuclei with 32.1 kg of NaI (TI) crystals in the Canfranc Underground Laboratory recording data along about 2 yr. A detailed description of the experimental setup, calibration procedure, and background analysis, including MC simulations, is presented. By comparing the observed direct spectrum (corresponding to 4613.6 kg day of exposure) with expectations, bounds on the properties of hypothetical particle dark matter candidates have been derived. The influence of the background modeling on these bounds is also discussed. Looking for an identifying signature of the WIMP's, we have observed the behavior of the data in the months of June and December of the 2 yr trying to find the differences implied by the rotation of the Earth around the Sun. No difference has been observed but, from the absence of such a modulation effect, constraints on masses and cross sections of spin-dependent and spin-independent interactions of WIMP's more restrictive than those obtained from the total rate have been found. The improvement on the sensitivity of residual spectrum versus total spectrum techniques in our experiment, as expected from the standard arguments, is clearly illustrated in this paper.

ACKNOWLEDGMENTS

The financial support of the Spanish Scientific and Technological Agency, CICYT, under Grant No. AE95-0747 is acknowledged.

[1] C. Bacci *et al.*, Phys. Lett. B **293**, 460 (1992).
[2] P. F. Smith *et al.*, Phys. Lett. B **379**, 299 (1996).
[3] K. Fushimi *et al.*, Phys. Rev. C **47**, R425 (1993).
[4] A. Drukier *et al.*, Phys. Rev. D **33**, 3495 (1986).
[5] E. García *et al.*, in *The Dark Side of the Universe: Experimental Efforts and Theoretical Framework*, Proceedings of the International Workshop, Rome, Italy, 1993, edited by R. Bernabei and C. Tao (World Scientific, Singapore, 1994), p. 216.
[6] K. Freese *et al.*, Phys. Rev. D **37**, 3388 (1988).
[7] M. Goodman and E. Witten, Phys. Rev. D **31**, 3059 (1985).
[8] E. García *et al.*, Phys. Rev. D **51**, 1458 (1995).
[9] N. J. C. Spooner *et al.*, Phys. Lett. B **321**, 156 (1994).
[10] G. Gerbie, *10th Moriond Workshop on Weak and Exotic Phenomena*, France, 1990 (Editions Frontieres, Gif-sur-Yvette, 1990), pp. 469–480.
[11] R. Bernabei *et al.*, Phys. Lett. B **389**, 757 (1996).
[12] J. Engel, Phys. Lett. B **264**, 114 (1991).
[13] J. Ellis and R. A. Flores, Nucl. Phys. **B400**, 25 (1993).
[14] A. F. Pacheco and D. Strottman, Phys. Rev. D **40**, 2131 (1989); F. Iachelo *et al.*, Phys. Lett. B **254**, 220 (1991).
[15] D. O. Caldwell *et al.*, Mod. Phys. Lett. A **5**, 1543 (1990).
[16] D. Reusser *et al.*, Phys. Lett. B **255**, 143 (1991).
[17] A. Drukier *et al.*, in *TAUP'91*, Proceedings of the Second International Workshop on Theoretical and Phenomenological Aspects of Underground Physics, Toledo, Spain, 1991, edited by A. Morales *et al.* [Nucl. Phys. B (Proc. Suppl.) **28A**, 293 (1992)].
[18] M. Beck *et al.*, Phys. Lett. B **336**, 141 (1994).